Nuclear Inst. and Methods in Physics Research, A 1055 (2023) 168445

Contents lists available at ScienceDirect

Nuclear Inst. and Methods in Physics Research, A

journal homepage: www.elsevier.com/locate/nima

Full Length Article

Resistive plate chambers for precise measurement of high-momentum protons in short range correlations at R^{3}B

M. Xarepe [a,b,*], T. Aumann [c,d], A. Blanco [e], A. Corsi [f], D. Galaviz [a,b], H.T. Johansson [g], S. Linev [d], B. Löher [d], L. Lopes [e], J. Michel [h], V. Panin [d], D. Rossi [c,d], J. Saraiva [e], H. Törnqvist [g], M. Traxler [d], for the R^{3}B collaboration

[a] Faculty of Science of the University of Lisbon, Lisbon, Portugal
[b] Laboratory of Instrumentation and Experimental Particle Physics, Lisbon, Portugal
[c] Darmstadt University of Technology, Department of Physics, Darmstadt, Germany
[d] GSI Helmholtz Centre for Heavy Ion Research, Darmstadt, Germany
[e] Laboratory of Instrumentation and Experimental Particle Physics, Coimbra, Portugal
[f] Department of Nuclear Physics, IRFU, CEA, Université Paris-Saclay, Paris-Saclay, France
[g] Chalmers University of Technology, Gothenburg, Sweden
[h] Goethe University Frankfurt, Frankfurt, Germany

ARTICLE INFO

Keywords:
Gaseous detectors
Timing
Time of flight
Resistive plate chamber
Short range correlations

ABSTRACT

The Reactions with Relativistic Radioactive Beams (R^{3}B) collaboration of the Facility for Antiproton and Ion Research (FAIR) in Darmstadt, Germany, has constructed an experimental setup to perform fundamental studies of nuclear matter, using as a probe reactions with exotic nuclei at relativistic energies. Among the various detection systems, one of the most recent upgrades consists of the installation of a large area, around 2 m^2, multi-gap Resistive Plate Chamber (RPC). The chamber is equipped with twelve 0.3 mm gaps and readout by 30 mm pitch strips, exhibiting a timing precision down to 50 ps and efficiencies above 98% for minimum ionizing particles in a previous characterization of the detector. The RPC was part of the setup of the FAIR Phase 0 experiment that focused on measuring for the first time, in spring 2022, nucleon–nucleon short-range correlations (SRC) inside an exotic nucleus (^{16}C). The excellent timing precision of this detector will allow the measurement of the forward emitted proton momentum with a resolution of around 1%. In beam measurements show an RPC efficiency above 95% and a time precision better than 100 ps (including the contribution of a reference scintillator and the momentum spread of the particles) for forward emitted particles.

1. Introduction

Understanding how the nuclear force acts on protons and neutrons inside a nuclear system is one of the hot topics in nuclear physics. At long distances, the attractive nuclear force is reasonably well modeled by ab-initio calculations based on realistic nuclear interactions and currents [1]. At short distances (below 1 fm) this force becomes strongly repulsive, giving rise to the appearance of nucleon pairs with very high relative momentum (above the Fermi level), a phenomenon known as Short-Range Correlations (SRCs) [2].

This characteristic of the strong nuclear force has been studied over the past years by the Continuous Electron Beam Accelerator Facility (CEBAF) Large Acceptance Spectrometer (CLAS) collaboration, [3] in high-energy electron scattering experiments using stable targets. One of their most relevant results indicates that the fraction of high-momentum protons increases with the neutron excess in the nucleus, see Fig. 1. This could have very strong implications in the description of high-density nuclear matter environments like neutron stars [4]. These correlated nucleon pairs are directly connected to the changes observed in the quark distribution in bound nucleons inside nuclei (the so-called EMC effect) [5]

As studies in stable nuclei do not allow to explore these effects at higher N/Z values, it is mandatory to orient the efforts towards exotic nuclear systems. However, reaction targets of radioactive isotopes are not available at N/Z > 1.5, and thus reaction studies need to be performed in inverse kinematics.

Along this line, a first SRC study using inverse kinematics was carried out in Dubna by the Baryonic Matter @ Nuclotron-based Ion Collider fAcility (NICA) (BM@N) collaboration, [6]. In this experiment, a stable beam of ^{12}C, with an energy of 3.2 AGeV, collided against a proton target, studying the ^{12}C(p,2p)X reaction. By measuring the

* Corresponding author at: Faculty of Science of the University of Lisbon, Lisbon, Portugal.
E-mail address: mxarepe@lip.pt (M. Xarepe).

https://doi.org/10.1016/j.nima.2023.168445
Received 11 December 2022; Received in revised form 21 April 2023; Accepted 23 April 2023
Available online 15 June 2023

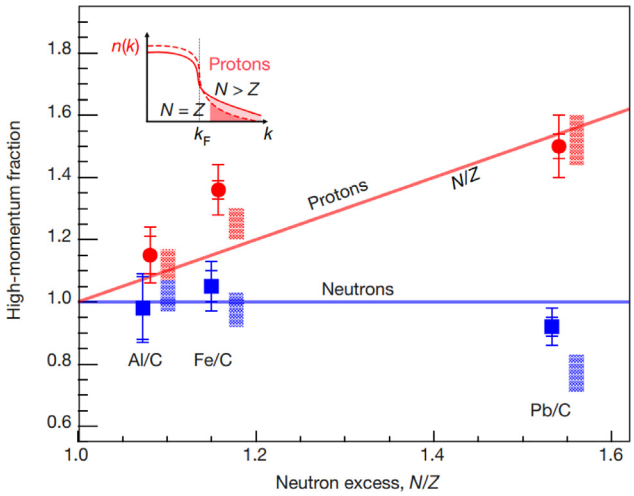

Fig. 1. The relative high-momentum fraction for neutrons (in blue squares) and protons (in red circles). The red and blue rectangles show the range of predictions of the phenomenological np-dominance model for proton and neutron ratios, respectively. The red line (high momentum fraction equal to N/Z) and the blue line (high-momentum fraction equal to 1) are drawn to guide the eye [3].

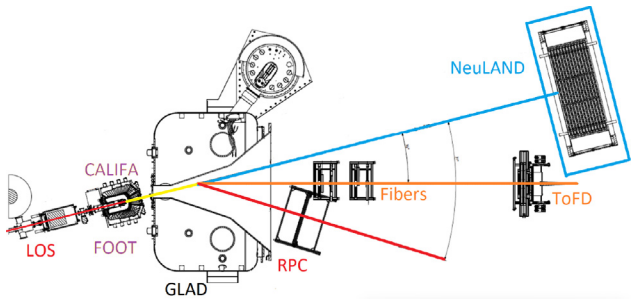

Fig. 2. Schematic view of R^{3}B collaboration experimental setup considered for the measurement of SRCs in inverse kinematics.

emitted nucleons in coincidence with the residual nuclei ^{11}B and ^{10}Be, a limited but significant amount of SRC events were observed, paving the path towards experiments with radioactive beams using similar reaction kinematics.

As such, the Reactions with Relativistic Radioactive (R^{3}B) collaboration of the upcoming Facility for Antiproton and Ion Research (FAIR) has designed and constructed an experimental setup. This setup enables the complete characterization of the reaction products from collisions of unstable radioactive beams on a liquid hydrogen target, allowing exclusive measurement of the A(p,2pN)A-2 reaction.

Fig. 2 shows the experimental setup designed by the R^{3}B collaboration for this type of measurement, from left to right in the beam direction: a fast scintillator (LOS) for measuring the start time of the reaction, the CaLorimeter for In-Flight detection of gamma rays and high-energy charged pArticles (CALIFA), silicon-based detector (FOOT) for reconstructing the reaction vertex, the GSI Large Acceptance Dipole (GLAD), a superconducting magnet, a scintillator fiber tracker (Fibers), and a scintillator (TOFD) measuring the outgoing heavy fragment, the new Large-Area Neutron Detector (NeuLAND) for the neutron Time-Of-Flight (TOF) determination, and a Resistive Plate Chamber (RPC) for the proton TOF detection.

The RPC detector has been the latest to be incorporated the R^{3}B setup with the objective of precisely measuring, by means of the TOF technique, the momentum of the protons emitted in the forward direction.

This detector has been previously characterized, achieving a time and position precision of around 50 ps and approximately 1 cm^2 for

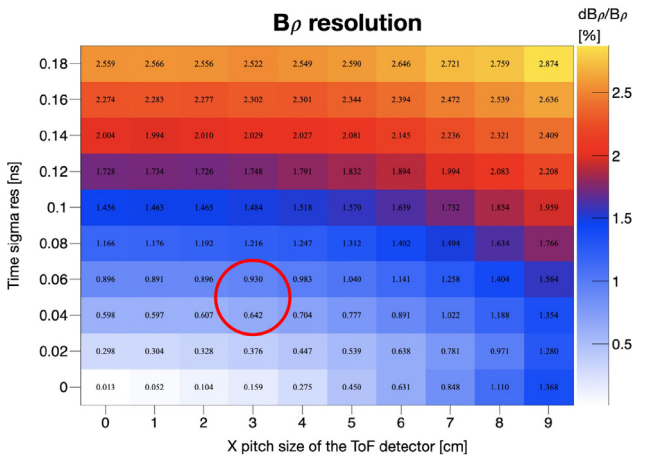

Fig. 3. Resolution of the B$\rho = p/e$ reconstruction considering different detector characteristics. The proposed RPC will be located in the region delimited by the red circle, with a resolution better than 1%.

Minimum Ionizing Particles (MIPs) [7]. All the time precisions presented in this work are obtained as sigma of a Gaussian fit to the distribution. A study based on simulations shows that such a detector will allow the measurement of the momentum of forward emitted protons with a resolution better than 1%. This result is shown in Fig. 3, where the resolution of the rigidity, B$\rho = p/e$, where B is the magnetic field of GLAD, ρ the radius of curvature, p the proton momentum and e the electron charge, is shown as a function of time resolution and pitch size. The performance level of the RPC detector proposed here corresponds to the region delimited by the red circle.

This setup was used for the first time in May 2022 to measure SRC in reactions of a ^{16}C radioactive beam, with an energy of 1.25 AGeV, on a liquid-hydrogen target. This article concentrates on the characteristics of the RPC detector used, its calibration procedure and the first results.

2. The RPC system on the R^{3}B setup

The RPC detector consists of two multigap RPC [8] modules, each of them confined in a permanently sealed plastic[1] gas tight box equipped with feed-throughs for gas and High Voltage (HV) connections. Each RPC module has six gas gaps defined by seven 1 mm thick float glass[2] electrodes of about 1550 × 1250 mm^2 separated by 0.3 mm nylon monofilaments. The HV electrodes are made up of a semi-conductive layer[3] applied to the outer surface of the outermost glasses with airbrush techniques.

The two modules are read out in parallel by a readout strip plane[4] equipped, in one side, with 41 copper strips (29 mm width, 30 mm pitch, and 1600 mm long) located in between the two modules. Two ground planes, located on top and bottom of the two-module stack, complete the readout planes. The complete structure is enclosed in an aluminum box that provides the necessary electromagnetic insulation and mechanical rigidity. In Fig. 4 a schematic of the inner structure of the module is shown.

Strips are read from both sides by fast Front End Electronics (FEE) [9]. These are capable of encoding in a single output signal: time (leading edge), with precision <30 ps and charge (pulse width). The charge is obtained by measuring the Time over Threshold (T_{ToT}) on a copy of the amplified signal, integrated with an integration constant

[1] Poly(methyl methacrylate) (PMMA) for the frame and Polycarbonate (PC) for the covers.

[2] Bulk resistivity of $\approx 4 \times 10^{12}$ Ω cm at 25 °C.

[3] Based on an artistic acrylic paint with around 100 MΩ/□.

[4] Made of 1.6 mm Flame Retardant 4 (FR4) Printed Circuit Board (PCB).

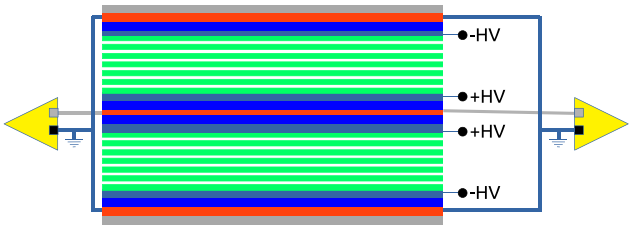

Fig. 4. Schematic of the internal structure of the of RPC detector (not to scale). Gray — Aluminum box. Red — Readout electrodes. Blue — Plastic tight box. Black — HV electrodes. Green-Glass Electrodes. Yellow triangles — FEE.

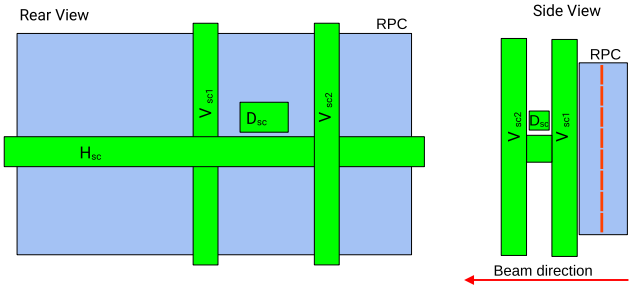

Fig. 5. Schematic of the positioning of the scintillator behind the RPC, rear view on the left and side view on the right.

of approximately 100 ns. The resulting signals are read out by a TDC-and-Readout Board (TRB) [10], version 3, equipped with 128 multihit Time-to-Digital Converter (TDC) channels (TDC-in-FPGA technology) with a time precision better than 20 ps. This board together with a TRB, version 3sc working as a logic unit and trigger distribution, constitute an autonomous DAta acQuisition (DAQ) system that exports data and synchronizes, via white rabbit protocol, with the R^{3}B DAQ system.

The RPC was operated in an open gas loop with a mixture of 98% $C_2H_2F_4$ and 2% SF_6 at a pressure a few millibars below atmospheric pressure. In this way, the width of the gaps is correctly defined as a result of the compression, several kg, exerted by the atmospheric pressure, not requiring mechanical compression. The detector working point was measured to be about 3000 kV/gap.

Three scintillation bars [11], two verticals, V_{sc1} and V_{sc2} and one horizontal, H_{sc} together with a small, 80 mm long, scintillator, D_{sc}, were placed behind and parallel to the surface of the RPC, as shown in Fig. 5, for calibration purposes. The scintillators are read out on both sides by photomultiplier tubes (PMT), the output signals of which are connected to the same FEE that reads the RPC but without the amplification stage.

For each RPC strip, i, with signals on both sides, the T_{ToT} measured on the right and left sides, $T_{\mathrm{ToT},r,i}$ and $T_{\mathrm{ToT},l,i}$ are corrected with a calculated offset associated with each of the FEE and TDC involved, $\epsilon_{\mathrm{ToT},r,i}$ and $\epsilon_{\mathrm{ToT},l,i}$. Computing in this way the charge of each channel,

$$\begin{aligned} Q_{r,i} &= T_{\mathrm{ToT},r,i} + \epsilon_{\mathrm{ToT},r,i} \\ Q_{l,i} &= T_{\mathrm{ToT},l,i} + \epsilon_{\mathrm{ToT},l,i} \end{aligned} \tag{1}$$

Furthermore, the strip, I, with maximum $Q_{r,i}$ and $Q_{l,i}$, will be the assigned strip of the event and the charge, Q, can be calculated from $Q_{r,I}$ and $Q_{l,I}$ as follows.

$$Q = \frac{Q_{r,I} + Q_{l,I}}{2} \tag{2}$$

Having assigned a strip to the event, the transversal position (across the strips), Y, can be computed using the number of the strip I and the pitch of the strip, w,

$$Y = (I - 1) \times w \tag{3}$$

For both the time T and the longitudinal position (along the strip) X, the measured times on the right and left sides of the selected strip will be used, $T_{r,I}$ and $T_{l,I}$ respectively, being that for each of these variables an offset must be calculated, $\epsilon_{T,I}$ and $\epsilon_{X,I}$.

To calculate the longitudinal position, X, Eq. (4) is used, where V_{strip} is the propagation velocity of the signals on the strips equal to 165.7 mm/ns.

$$X = \left[\frac{(T_{r,I} - T_{l,I})}{2} \times V_{\mathrm{strip}} \right] + \epsilon_{X,I} \tag{4}$$

For time T Eq. (5) is used.

$$T = \frac{(T_{r,I} + T_{l,I})}{2} + \epsilon_{T,I} \tag{5}$$

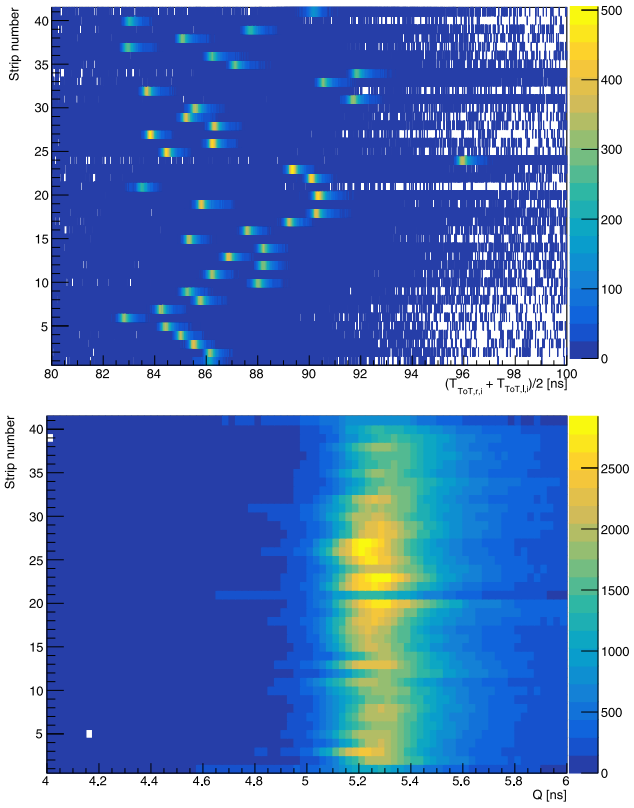

Fig. 6. (Top), $(T_{\mathrm{ToT},r,i} + T_{\mathrm{ToT},l,i})/2$ and (bottom), Q for all strips.

3. Calibration

The calibration of the RPC is done in a few steps.

3.1. Time over threshold calibration

The calibration of the T_{ToT} consists of the calculation of the $\epsilon_{\mathrm{ToT},r,i}$ and $\epsilon_{\mathrm{ToT},l,i}$ parameters, originated from the different response of each of the FEE and TDC channels involved. The parameters align the minimum value of $T_{\mathrm{ToT},r,i}$ and $T_{\mathrm{ToT},l,i}$ between all channels. This calibration is crucial for the determination of $Q_{r,I}$ and $Q_{l,I}$ with the consequent correct calculation of Q, T, Y and X.

If this calibration is not performed correctly, $Q_{r,I}$ and $Q_{l,I}$ could be attributed to different channels on the left and right sides, in which case the event would be discarded or attributed to the wrong strip. This is visible in Fig. 6 top, where the uncalibrated $(T_{\mathrm{ToT},r,i} + T_{\mathrm{ToT},l,i})/2$ spectra are plotted for each of the strips. Due to the lack of calibration, 10% of the events will be discarded. After a correct calibration, Fig. 6 bottom, the value of events with incorrect Q decreases to 2%. More work is being done to further improve this value.

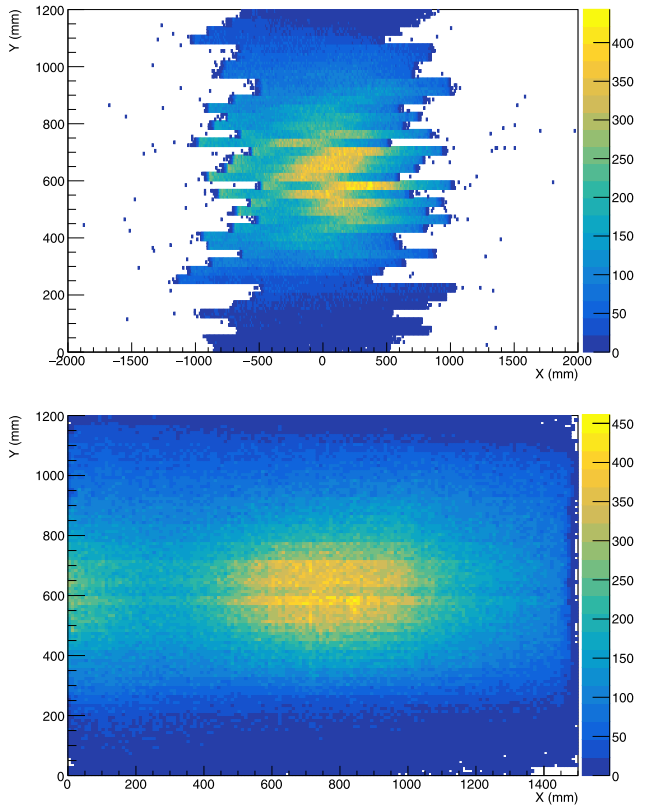

Fig. 7. X, Y map before (Top) and after (Bottom) applying calibration parameter $\epsilon_{X,I}$. The central spot corresponding to the forward emitted particles (protons) and the geometrical acceptance defined by the GLAD magnet (halo at the periphery of the plot) are clearly visible in bottom plot.

3.2. Longitudinal strip position calibration

After a correct calibration of the T_{ToT} and calculation of Q, the transverse and longitudinal positions, Y and X, are calculated. For the latter, it is necessary to determine the parameters $\epsilon_{X,I}$, which have as origin the different time offsets associated with the FEE and TDC channels of each strip.

This is visible in Fig. 7 top, where a two-dimensional histogram of Y, X, without the calibration parameters, is shown. In contrast, Fig. 7 bottom shows the same histogram with the calculated calibration parameters, where the central spot corresponding to the forward emitted particles (protons) and the geometrical acceptance defined by the GLAD magnet (halo at the periphery of the plot) are clearly visible.

3.3. Strip time calibration

Finally, the time T, can be determined, for which the parameters $\epsilon_{T,I}$ must be calculated, which have as origin the different time offsets associated with the FEE and TDC channels of each strip.

The vertical scintillators are used to calculate these parameters.

For each of the strips, the differences are calculated between the scintillator time and the RPC time, $T_{sc1} - T$ (for the case of the scintillator V_{sc1}). Assuming that the scintillators are perfectly parallel to the surface of the RPC, the time of flight for the particles between the two detectors should be, on average, equal, without depending on the strip of the RPC that has produced the signal. Therefore, the parameters $\epsilon_{T,I}$ are calculated such that the average of $T_{sc1} - T$ is always the same.

The result can be seen in Fig. 8, where $T_{sc1} - T$, is calculated for each of the strips . In the top part without the calibration parameters and at the bottom with the calculated calibration parameters applied. This procedure ensures that the RPC surface always produces the same time regardless of the strip producing the signal.

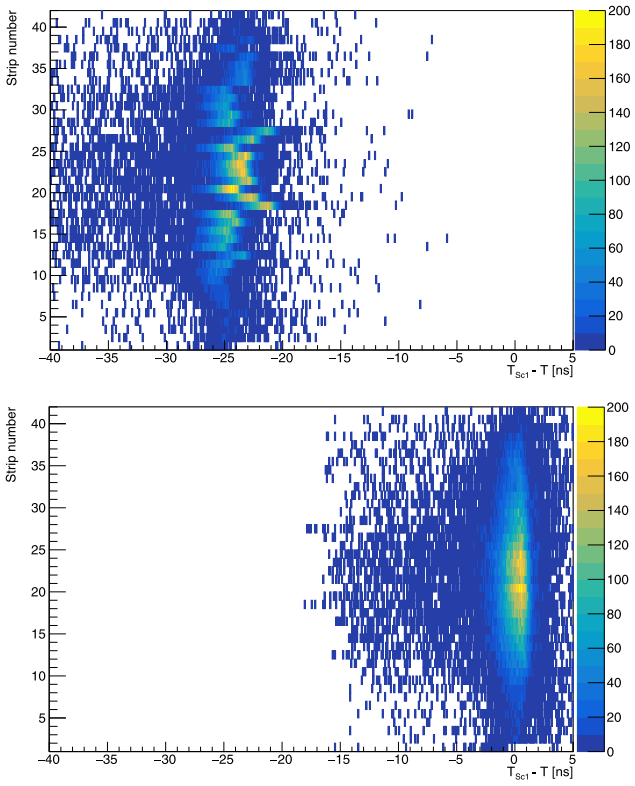

Fig. 8. Top, $T_{sc1} - T$ difference without calculation of $\epsilon_{T,I}$ parameters and with calculated ones in bottom.

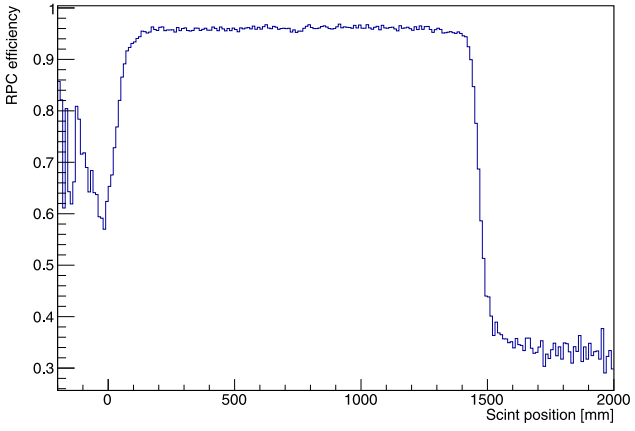

Fig. 9. Beam time efficiency. Estimated efficiency of the RPC as a function of the H_{sc} longitudinal position placed behind the RPC, showing an average value of around 95%.

4. Beam time performance

The RPC autonomous DAQ system ran without interruption for more than two weeks, delivering data and correctly synchronizing with the R^3B DAQ.

Using the horizontal scintillator, H_{sc}, the efficiency was calculated on the overlapped area. It was estimated by dividing the events seen by the LOS, RPC and H_{sc} by all the events seen by the LOS and H_{sc} detectors. The result can be seen in Fig. 9 where the efficiency of the RPC is shown as a function of the position given by the scintillator, showing a mean value of 95%.

The time precision of the RPC was estimated by performing the time difference between the RPC and the small scintillator (D_{sc}), which has the best time precision of the four scintillators. Fig. 10 shows the time

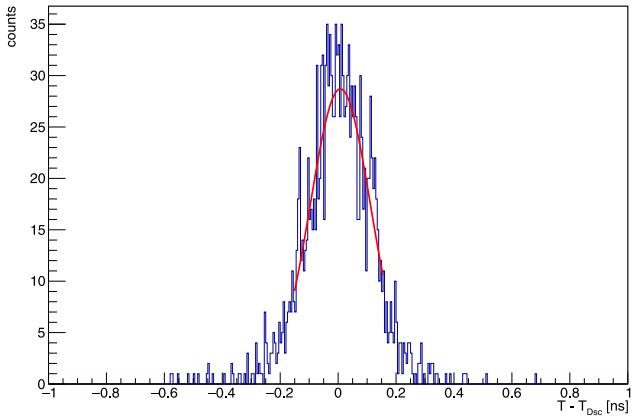

Fig. 10. Time difference between the RPC and the small scintillator (D_{sc}) showing a sigma of ≈100 ps after fitting the central Gaussian part of the distribution.

difference $T - T_{Dsc}$, which after fitting the central Gaussian part of the distribution shows a value of 100 ps. This value includes the precision of the RPC, D_{sc}, and the spread in momentum of the particles. In a previous characterization with a collimated monochromatic relativistic pion beam, the precision of D_{sc} was evaluated to be around 35 ps. As these conditions are not met here, its contribution to the time resolution is probably higher. The contribution of momentum has been calculated to be negligible for the distance between RPC and D_{sc} based on the measured TOF between LOS and RPC.

5. Conclusions

The setup (installation, DAQ integration and calibration) of a large area, 2 m^2, RPC detector for the precise momentum measurement of forward emitted protons in collisions of unstable radioactive beams on a liquid hydrogen target has been successfully done. During the first beam time, the RPC exhibited an efficiency higher than 95% and a time precision better than 100 ps.

Declaration of competing interest

The authors declare that they have no known competing financial interests or personal relationships that could have appeared to influence the work reported in this paper.

Acknowledgments

This work was supported by Fundação para a Ciência e Tecnologia (FCT), Portugal, within the framework of the project EXPL/FIS-NUC/0364/2021 and the PhD grant 2021.05736.BD.

References

[1] J. Carlson, et al., Quantum Monte Carlo methods for nuclear physics, Rev. Modern Phys. 87 (2015) 1067.
[2] V.V. Burov, et al., Large momentum pion production in proton nucleus collisions and the idea of fluctuons in nuclei, Phys. Lett. B 67 (1977) 46.
[3] The CLAS Collaboration, Probing high-momentum protons and neutrons in neutron-rich nuclei, Nature 560 (2018) 617–621.
[4] L.A. Souza, et al., Effects of short-range nuclear correlations on the deformability of neutron stars, Phys. Rev. C 101 (2020) 065202.
[5] Or. Hen, et al., Nucleon–nucleon correlations, short-lived excitations, and the quarks within, Rev. Modern Phys. 89 (2017) 045002.
[6] M. Patsyuk, et al., Unperturbed inverse kinematics nucleon knockout measurements with a carbon beam, Nat. Phys. 17 (6) (2021) 693–699.
[7] A. Blanco, et al., The ship timing detector based on MRPC, J. Instrum. (2020) C10017.
[8] E. Cerron Zeballos, et al., A new type of resistive plate chamber: The multigap RPC, NIMA 374 (1) (1996) 132–135.
[9] D. Belver, et al., Performance of the low-jitter high-gain/bandwidth front-end electronics of the HADES tRPC wall, TNS 57 (5) (2010) 2848–2856.
[10] A. Neiser, et al., TRB3: a 264 channel high precision TDC platform and its applications, J. Instrum. 8 (12) (2013) C12043.
[11] K. Boretzky, et al., NeuLAND: The high-resolution neutron time-of-flight spectrometer for R3B at FAIR, NIMA 1014 (2021) 165701.